Modified Ionospheric Correction Algorithm for the SBAS Based on Geometry Monitor Concept

Takeyasu Sakai, Keisuke Matsunaga, and Kazuaki Hoshinoo, *Electronic Navigation Research Institute, Japan*
Todd Walter, *Stanford University, USA*

BIOGRAPHY

Takeyasu Sakai is a Senior Researcher of Electronic Navigation Research Institute, Japan. He received his Dr. Eng. in 2000 from Waseda University and is currently analyzing and developing ionospheric algorithms for Japanese MSAS program. He is a member of the MSAS Technical Review Board of JCAB.

Keisuke Matsunaga is a Researcher of Electronic Navigation Research Institute. He received his M. Sc. in 1996 from Kyoto University and worked for the development of LSI at Mitsubishi Electric Corporation from 1996 to 1999. He joined ENRI in 1999, and is currently studying ionospheric scintillation effects on MSAS. He is a member of the MSAS Technical Review Board of JCAB.

Kazuaki Hoshinoo is a Principal Researcher of Electronic Navigation Research Institute. He is the director of MSAS research program in ENRI and is a member of the MSAS Technical Review Board of JCAB. He chairs Ionosphere Working Group of the Board.

Todd Walter is a Senior Research Engineer in the Department of Aeronautics and Astronautics at Stanford University. Dr. Walter received his PhD. in 1993 from Stanford and is currently developing WAAS integrity algorithms and analyzing the availability of the WAAS signal.

ABSTRACT

The ionospheric correction procedure of the current MSAS, Japanese version of SBAS/WAAS, is built on the algorithm called as 'planar fit'. It estimates the ionospheric propagation delays at IGPs using the first order estimator, relates to 'plane', and the storm detector is implemented to determine if there is storm condition or not to protect users from large correction errors. The previous study has shown that the algorithm works relatively well over Japan although the absolute delay is large due to geomagnetic effects.

A potential problem is, however, the fact that the distribution of residual errors after planar fit removal is not Gaussian, which is assumed in the storm detector algorithm of MSAS/WAAS. During storm conditions, the availability of ionospheric corrections for MSAS tends to lower significantly due to trip of storm detector even the actual error is small.

Another problem is that the current storm detector determines ionospheric conditions based on the observed residuals. This approach, dependent upon observations, cannot avoid undersampling threat; We never observe where observation does not exist. In fact, chi-square statistics implicitly expects a good geometry of observations. A small chi-square value does not guarantee that the actual error distribution is normal due to a possible undersampling situation.

The authors will introduce geometry monitor concept to overcome these problems. Using an appropriate metric indicating goodness of the geometry of observations, it is possible to bound the actual error by a function of the metric. The relative centroid metric (RCM) and condition number metric (CNM) are evaluated for this purpose. These metrics can also be applied to determine which model, or the order of fit, is better for fit. Employing an adaptive fit algorithm based on the geometry monitor, the availability of the ionospheric corrections improves from 70-80% to over 99%. Missed detection conditions are eliminated with little enlargement of GIVE values.

INTRODUCTION

Japan has been developing its own satellite-based GPS augmentation system called MSAS (MTSAT satellite-based augmentation system) since 1993 [1]. The MSAS is developed primarily for civil aviation purpose so it shall broadcast radiosignal based on the international standard

developed and defined by ICAO (international civil aviation organization). SBAS (satellite-based augmentation system) is ICAO standard of the wide area augmentation system which augments GPS using additional signals transmitted from geostationary satellites [2][3]. As an international standard system, Japanese MSAS is compatible with US WAAS and European EGNOS. SBAS receiver shall work with any of these systems.

Following the failure of MTSAT-1 launch in 1999, MTSAT-1R geostationary satellite was successfully launched in February 2005. MTSAT means multi-functional transport satellite, because it has weather and aviation missions. For aviation users, MTSAT provides transponder channels both of satellite communications including the automatic dependent surveillance (ADS) function as well as voice, and MSAS navigation datalink. MTSAT-1R is functional on the geostationary orbit at 140E and, so far, MSAS is under test procedures.

The major problem for SBAS is the ionosphere. The SBAS ionospheric correction messages and procedure defined in SARPs documents [2] were actually developed based on the observation and knowledge on the ionospheric activities over the US CONUS. In fact, the ionosphere has the significant activities in the equatorial regions in contrast to a case of CONUS located in the relatively high magnetic latitude region. The equatorial anomalies affect as the large-scale structure of electron density of ionosphere which might be difficult to be eliminated by SBAS ionospheric correction messages [4]-[6]. Plasma bubble effects (also known as depletion), usually occur also in the low latitude region, might cause significant scintillation which disrupts GPS signals [7]-[10].

The ionospheric delay problem is currently the largest concern for MSAS program. In early 2004 the MSAS Technical Review Board of JCAB (Japan Civil Aviation Bureau) established an Ionosphere Working Group for this problem. Supporting such activities, the authors are investigating the ionospheric effects over Japan to predict and improve the actual performance of MSAS on the ionosphere.

The authors have already introduced quadratic fit in order to improve correction performance and zeroth fit for better availability of ionospheric corrections [6]. Zeroth order fit can be performed even only a few measurements are available, so it can save 5-6 percent of IGPs during a severe ionospheric condition such as October 2003 storm. Second order fit, *i.e.*, quadratic fit, can improve the estimation accuracy up to 12 percent in RMS sense, with a good geometry of IPP measurements.

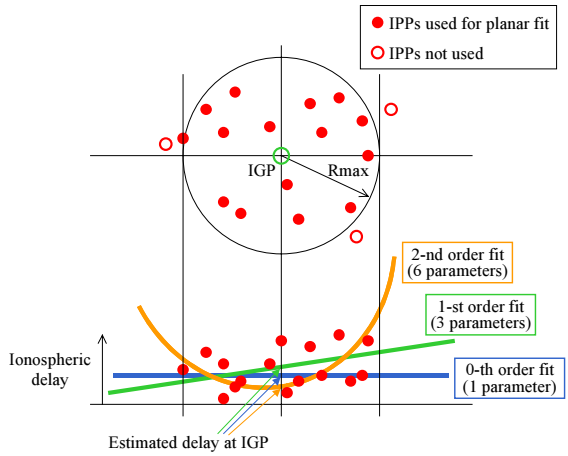

Figure 1. Planar fit algorithm for SBAS ionospheric delay estimation. The current algorithm is the first order planar fit.

In this paper the authors will firstly review the performance of the current planar fit algorithm for the SBAS over Japan. The potential problem here is the fact that the distribution of residual errors of planar fit is not Gaussian. The current storm detector based on chi-square statistics does not work well in such conditions, leading quite a lot of false alarm conditions and, more significantly, missed detection conditions.

Another problem is that the current storm detector determines ionospheric conditions based on the distribution of observed residuals. This approach relies on observations, so cannot avoid undersampling threat. In fact, chi-square statistics implicitly expects a good geometry of observations. A small chi-square value does not guarantee that the actual error distribution is Gaussian, or normal, due to a possible undersampling situation.

The authors will introduce geometry monitor concept to overcome these problems. Our original purpose is not to identify cases of storm conditions; It is just necessary to control GIVE values to bound actual user errors within the associate protection level regardless if there is a storm condition or not. If there is possibility that the ionosphere causes a large user error, the MCS must set large GIVE values to protect users even there is no storm condition.

Using an appropriate metric indicating goodness of the geometry of observations, it is possible to bound the actual error by a function of the metric. The relative centroid metric (RCM) and condition number metric (CNM) are evaluated for this purpose. These metrics can also be applied to determine which model is better for fit. Employing an adaptive fit algorithm based on the geometry monitor, the availability of the ionospheric corrections improved from 70-80% to over 99%. Missed detection conditions are eliminated with little enlargement of GIVE values.

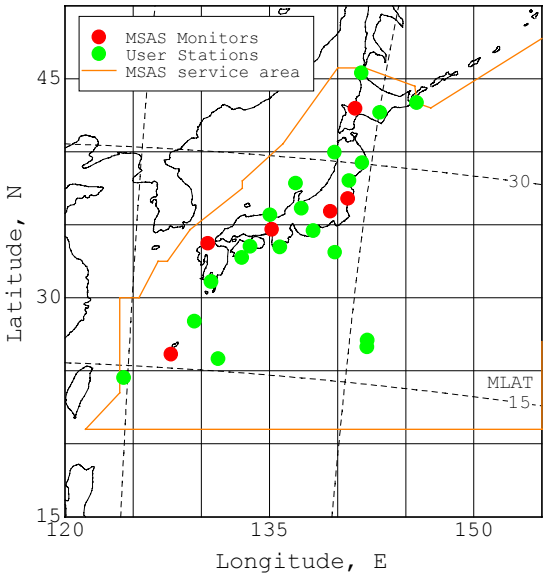

Figure 2. Distribution of observation sites for the dataset.

STANDARD PLANAR FIT FOR SBAS

First of all, let us review the performance of the standard planar fit within the service area of the MSAS. Here we employ the planar fit procedure explained in [11].

The dataset of ionospheric delay observations during both quiet and stormy geomagnetic conditions are prepared for this purpose. Data source is GEONET network operated by Japan's Geographical Survey Institute, which equips over a thousand stations distributed in Japan. All stations in the network have dual-frequency survey-grade GPS receivers and provide their measurements at every 30 seconds in the RINEX format. Pseudorange observations at 26 stations are converted into ionospheric delay dataset with removal of interfrequency biases [12][13]. Note that the dataset is based on only code phase pseudorange measurements instead of ambiguous carrier phase measurements, in order to avoid any ambiguities and cycle slips corrupting ionospheric analysis. Time-domain smoothing filter were applied to reduce multipath errors.

Figure 2 shows the distribution of observation stations involved in the dataset. Note that all stations used in this analysis belong to the GEONET. Evaluating the performance of planar fit, the dataset was divided into two parts; (i) IPP measurements: observations measured by MSAS-like 6 stations (Monitor Stations; red stations in Figure 2) are used as IPPs for generating fitting 'plane'; and (ii) IGP measurements: observations at the other 20 stations (User Stations; green stations in Figure 2) are used as pseudo-IGPs for evaluating how the 'plane' is good or bad, so never used as estimation sources. Because SBAS must bound the user positioning error at any (unknown) user location, we need to evaluate its performance using these User Stations which provide true measurements at the pseudo-IGPs, other than Monitor Stations. Planar fit was performed at each pseudo-IGP and evaluated by the difference between the 'plane' and true measurement at the pseudo-IGP (called 'residual'). Hereinafter, IPP and IGP represent Monitor and User measurements, respectively, as described here.

Using planar model, the vertical ionospheric delay at an IGP is estimated by [11]:

$$\begin{bmatrix} \hat{a}_0 & \hat{a}_1 & \hat{a}_2 \end{bmatrix}^{\mathrm{T}} = \left(G^{\mathrm{T}} \cdot W \cdot G \right)^{-1} \cdot G^{\mathrm{T}} \cdot W \cdot \mathbf{I}_{\mathbf{v,IPP}}, \qquad (1)$$

where G is $N \times 3$ design matrix which describes the geometry of IPPs, and W^{-1} is the covariance matrix of the observation set, $\mathbf{I}_{\mathbf{v,IPP}}$. $\hat{I}_{v,IGP} = \hat{a}_0$ is the resulted estimation and thus residual error is given by $\delta_{v,IGP} = I_{v,IGP} - \hat{I}_{v,IGP}$. Note that we have the true delay $I_{v,IGP}$ as the user measurement in this analysis but do not for real system.

Figure 3 represents a histogram plot of residual errors for all user measurements during November 2004 storm. RMS of residual error was 0.982 meter while the largest error was 20.1 meters. Large errors below –10 meters occurred on the southern ocean near the edge of the MSAS service area. Such a histogram is typical during severe storms.

The Current Storm Detector

Integrity is the most important requirement for SBAS, so the bounding information of corrected pseudoranges is broadcast to users. For ionospheric corrections, the MCS broadcasts GIVE value for this purpose. The current algorithm computes GIVE values based on the formal variance of the least square fit with the assumption that the distribution of residual errors is normal, so it needs to determine whether each IGP is in storm condition or not. The 'storm' condition means the distribution of residual errors is possibly not normal.

The formal variance of the least square fit of Eqn. (1) is given by:

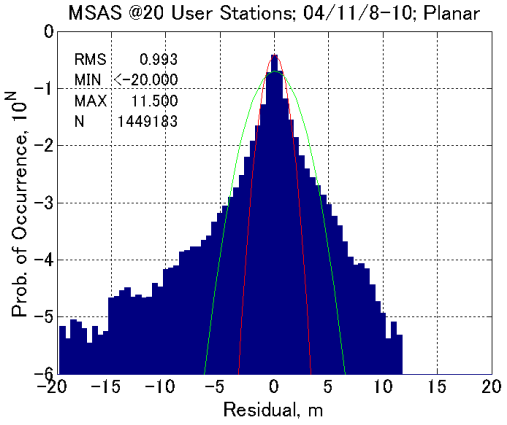

Figure 3. Histogram plot of the residual errors of planar fit during November 2004 storm. No storm detector applied.

$$\hat{\sigma}^2_{\hat{I}_{v,IGP}} = \left[\left(G \cdot W \cdot G^{\mathrm{T}}\right)^{-1}\right]_{1,1}, \qquad (2)$$

and the bounding variance at the IGP is:

$$\hat{\sigma}^2_{bound,IGP} = \sqrt{\frac{\chi^2_{1-P_{FA}}}{\chi^2_{P_{MD}}}} \cdot \left(\hat{\sigma}^2_{\hat{I}_{v,IGP}} + \sigma^2_{decorr}\right), \qquad (3)$$

where a coefficient outside blanket is so-called inflation factor, and σ_{decorr} denotes inherent uncertainty of the fit plane. $\chi^2_p(n-3)$ is the thresholds for chi-square statistics as a function of the degree of freedom (the number of observations minus the number of unknowns). According to procedure to compute protection levels, defined by SARPs [2], the actual correction error must be bounded by $5.33\hat{\sigma}_{bound,IGP}$ anywhere and anytime. Now we can define the normalized residual error as:

$$\Delta_{v,IGP} = \delta_{v,IGP} \Big/ \hat{\sigma}_{bound,IGP} = \left(I_{v,IGP} - \hat{I}_{v,IGP}\right) \Big/ \hat{\sigma}_{bound,IGP} \cdot \qquad (4)$$

Clearly it gives an example that integrity of the system cannot be maintained if this normalized residual error exceeds 5.33 at somewhere in the service area.

The current storm detector determines whether an IGP is in storm condition or not based on the chi-square statistics of the observations,

$$\chi^2 = \left(\hat{\mathrm{I}}_{\mathrm{v,IPP}} - \mathrm{I}_{\mathrm{v,IPP}}\right)^{\mathrm{T}} \cdot W \cdot \left(\hat{\mathrm{I}}_{\mathrm{v,IPP}} - \mathrm{I}_{\mathrm{v,IPP}}\right), \qquad (5)$$

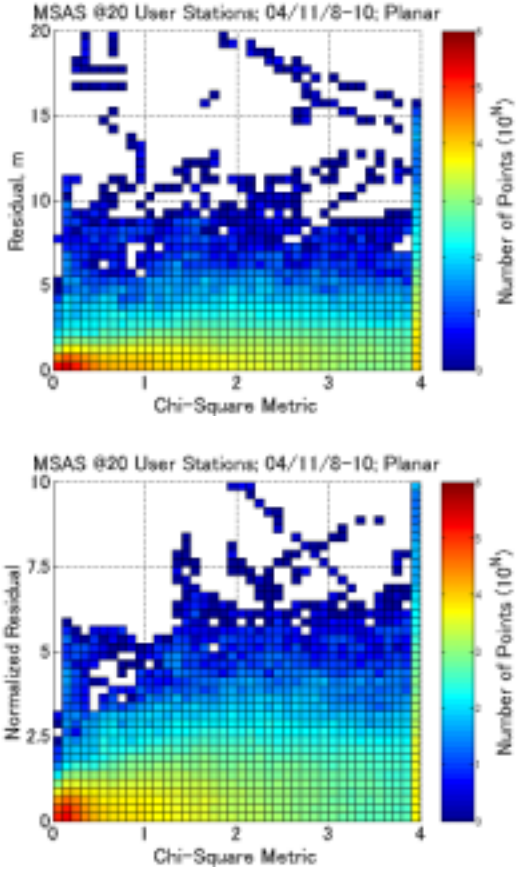

Figure 4. 2-D histogram plot representing the residual errors versus chi-square metric during November 2004 storm. Each IGP is determined as being storm state if the associate chi-square metric is greater than 1.

compared with the threshold, $\chi^2_{1-P_{FA}}(n-3)$. If chi-square statistics is larger than this threshold, the IGP is determined to be in storm condition and the associate GIVE value is set to the maximum in order to protect users from a possible large error.

If chi-square is less than the threshold, which means the IGP can be expected not in storm condition, SBAS computes the associate GIVE value by Eqn. (3). Note that, however, small chi-square does not guarantee that the actual error is bounded by the GIVE value, due to possible undersampling situation.

In fact, during a severe storm condition in November 2004, chi-square metric (chi-square statistics divided by the associate threshold) was distributed as shown in Figure 4. Each IGP is determined to be in storm condition if this metric is greater than 1. The missed detection condition occurred frequently with a large residual error which associates with chi-square metric less than 1, while

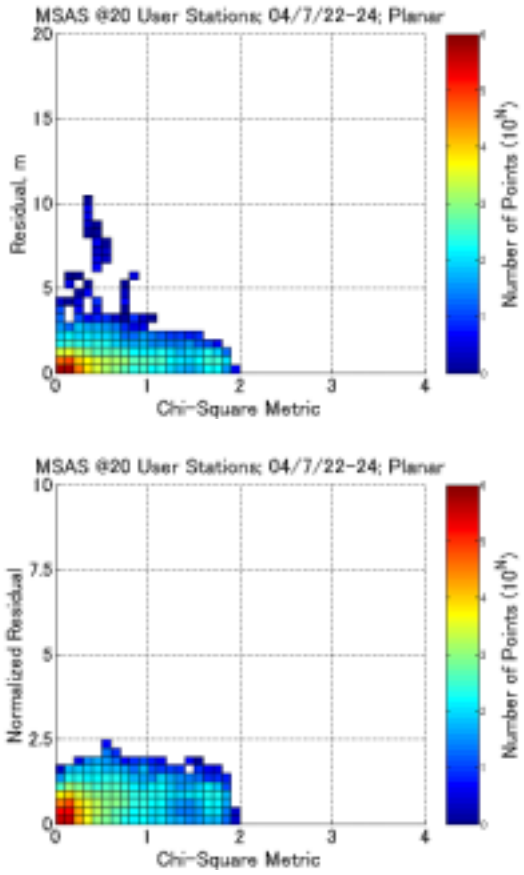

Figure 5. 2-D histogram plot representing the residual errors versus chi-square metric during active ionospheric condition. There are a lot of false alarm conditions.

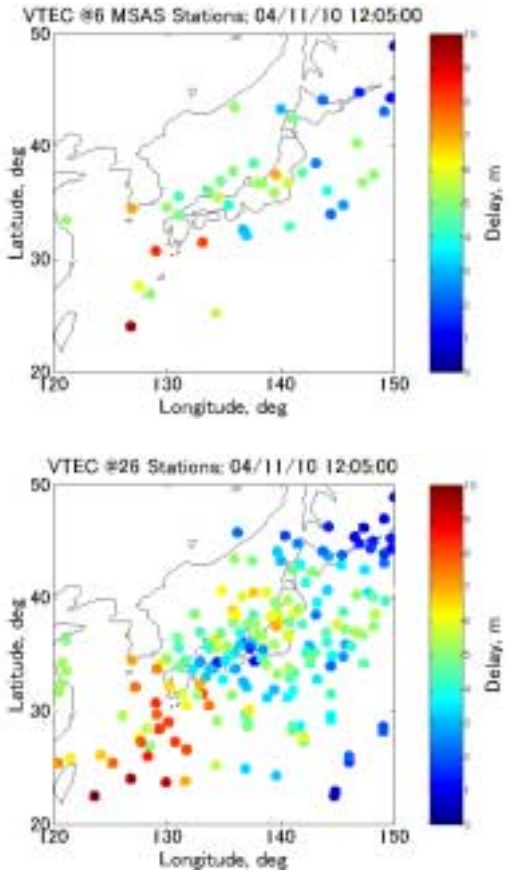

Figure 6. Ionospheric observations measured by (Upper) MSAS-like 6 monitor stations; and (Bottom) all 26 stations. Blue spots at the center of the bottom plot are not observed by MSAS-like stations.

a small residual error with chi-square metric greater than 1 means the false alarm condition. A missed detection condition threatens integrity of the system while the false alarm conditions lower availability of the system.

The variance computed by Eqn. (3) bounded the actual residual errors during the period other than severe storm, for example, as Figure 5 shows. However, there were a lot of false alarm conditions which sacrifice the availability of the system. Now we know that the current design of MSAS might be a kind of conservative.

Undersampling Problem

In the evaluation above, planar fit was performed only with Monitor measurement and resulted estimation of IGP vertical delay is compared with User measurements. Because there are only 6 Monitor stations in the service area of the MSAS, Monitor measurements are often sparse relatively to the mid-scale structure of ionosphere so ionosphere might not be well-sampled. One cannot detect any structures unless it is sampled.

Figure 6 displays a snapshot of the spatial distribution of ionospheric delays during November 2004 storm. Monitor stations observed smooth ionosphere (Top); But, in fact, there was mid-scale structure that some user stations certainly experienced (Bottom). Such unobservable structures may cause large errors leading missed detection conditions; This is the undersampling problem.

Unfortunately our storm detector cannot detect such a situation. The chi-square statistics does not reflect the geometry of IPPs. The chi-square statistics is actually a criteria for ‘sampled’ data but not for ‘sampling’ process. A chi-square test detects invalidity (not validity) of the assumption that the associate samples are taken from the population of normal distribution; It implicitly expects a good sampling geometry.

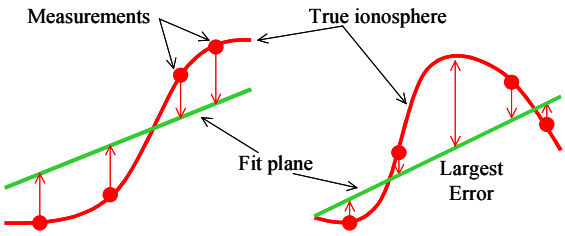

Figure 7. Two sampling situations; (Left) Well-sampled but large chi-square; (Right) under-sampled but small chi-square.

Figure 7 explains two sampling situations. A chi-square test can detect a situation such that the model for fit does not match to the actual ionosphere; The chi-square statistics becomes large with well-sampled observations. However, it might fail to detect undersampling situation such as shown in the right of the figure; The associate chi-square statistics can be small if the mid-scale structure is not sampled enough.

The fact is that we cannot observe 'hole' of IPP measurement distribution and never know what is there. There may be unobservable mountain, valley, or wave-like structure in any hole missing measurements but the MCS cannot capture them. Here is a threat against integrity of the system.

GEOMETRY MONITOR CONCEPT

One possible way to eliminate undersampling threat is monitoring the geometry of IPPs being used for fit based on the empirical knowledge. It is possible to assume a small correction error if IPPs are distributed with a good geometry, so that MCS can broadcast small GIVE value in order to maintain availability. Meanwhile, with poor geometry, the MCS cannot reduce GIVE value because there is a certain possibility that the associate correction information makes a large user error. This approach still arises false alarm conditions, but, at least, will reduce missed detection conditions due to undersampling.

The characteristics of the ionosphere around the service area must be well-characterized by off-line analysis of historical storm state observations. For this analysis, observations should not be limited to those collected by SBAS monitor stations because we must capture any structures threatening integrity of the system. GEONET network, which has a thousand sites in Japan at every 20-30 km separation and holds 30-second sampled observations for a decade, is quite useful for this type of analysis.

Some analyses have already been done and available [7][10][14]. It was reported that a gradient of vertical ionospheric delay up to 40 mm/km was observed during storm conditions [7]. And there was wave-like structure traveling from southwest to northeast [10]. A part of such structures might be captured by SBAS monitor stations but some of them would cause missed detection conditions with small chi-square statistics.

Recall that our original purpose is not to identify cases of storm conditions. It is necessary to control GIVE values to bound actual user errors within the associates protection level regardless if there is a storm condition or not. If there is possibility that the ionosphere cause a large user error, the MCS must set large GIVE values to protect users even there is no storm conditions.

The storm detector concept is built on the assumption that the distribution of correction errors is normal. This is actually a fact over US CONUS during geomagnetic quiet condition. The chi-square metric detects storm conditions which means this assumption is not valid. A large chi-square statistics implies possibility of a large user error, but a small chi-square statistics does not guarantee that the actual error is bounded by the GIVE value based on the formal variance, as Figure 4 says.

We need storm detector which determine if there is a storm condition or not because of the assumption that the distribution of residual error is normal. If there is an appropriate function bounding residual errors regardless if there is a storm condition or not, we do no longer need storm detector which lowers availability of the system. Such a function might be dependent only upon the geometry of the IPPs. Here the authors considered of two metrics indicating goodness of the geometry.

Relative Centroid Metric (RCM)

The relative centroid metric (RCM) [15] is the distance between IGP and weighted centroid of IPPs divided by planar fit radius. This metric is based only on the geometric distribution of IPPs used for fit, so independent from measured delays and the order of fit. Clearly, RCM varies between 0 and 1.

The weighted centroid is given by:

$$\lambda_{centroid} = \frac{\sum \lambda_{IPP,i} \cdot W_{ii}}{\sum W_{ii}}, \qquad (6)$$

$$\phi_{centroid} = \frac{\sum \phi_{IPP,i} \cdot W_{ii}}{\sum W_{ii}}, \qquad (7)$$

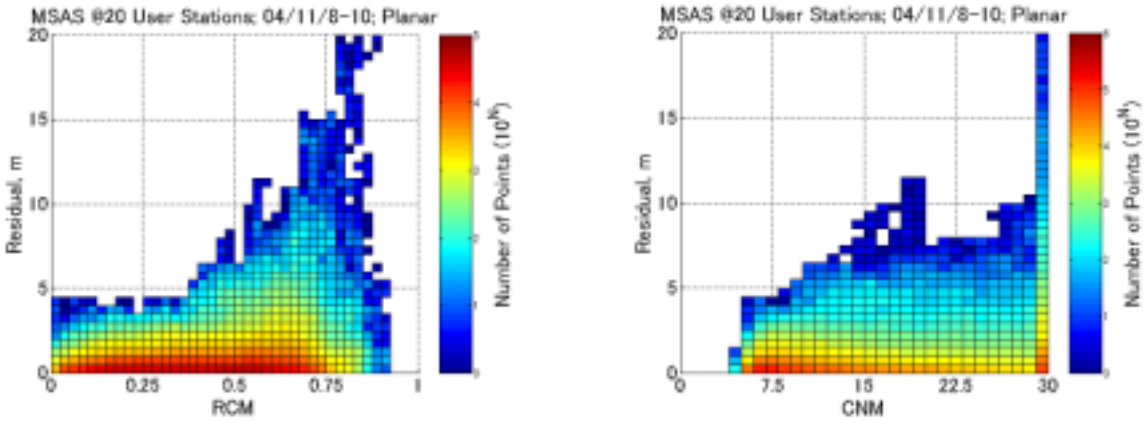

Figure 8. 2-D histogram plot representing the residual errors versus (Left) relative centroid metric; and (Right) condition number metric; during a severe storm. Compare with Figure 4.

where $\lambda_{IPP,i}$ and $\phi_{IPP,i}$ denote the longitude and latitude of the *i*-th IPP.

Figure 8 shows the distribution of residual errors with respect to the associate RCM. In contrast with case of chi-square metric shown in Figure 4, residual error is well-bounded if RCM is small. It is important fact that a large residual error is possible only if the RCM is greater than 0.5.

Condition Number Metric (CNM)

The authors have already introduced the condition number as a metric to determine the order of fit [5][6]. The condition number of a matrix is mathematically defined as the ratio of the largest singular value of the matrix to the smallest one. It is known that any linear equations can be solved by singular value decomposition (SVD) and the stability of the solution relates to the condition number of the design matrix, i.e., the left-hand-side of the equation.

Any matrix *A* can be decomposed into the form of:

$$A = U \cdot S \cdot V^T , \qquad (5)$$

where *S* is a diagonal matrix whose components are singular values of matrix *A*. The theory of SVD says that the equation $A\mathrm{x} = \mathrm{b}$ can be solved as $\mathrm{x} = VS^{-1}U^T \cdot \mathrm{b}$. Comparing with Eqn. (1), the design matrix *A* here is:

$$A = R^T \cdot G , \qquad (6)$$

where matrix *R* is Cholesky decomposition of matrix *W*, *i.e.*, $W = R \cdot R^T$. Note that matrix *G* has columns as many as the number of unknowns, 3 for the first order and 6 for the second, thus the condition number is dependent on both the geometry of IPPs and the order of fit. The number of singular values is also equal to the number of unknowns.

We can measure the stability of Eqn. (1) through the condition number obtained as $s_{\max} / s_{\min}$, *i.e.*, the largest singular value divided by the smallest. The estimated ionospheric delay might be unstable if the associate condition number is large. Eqn. (1) is formally over-determined if $N > 3$ for the first order fit, but at the same time it may be under-determined due to poor geometry of observations. For example, in case that all IPPs are distributed on one side of the IGP, Eqn. (1) becomes an extrapolation which might introduce a large error.

The condition number metric (CNM) is always positive up to 100 for the first order fit while becomes thousands for second order fit. Figure 8 also gives an example of the distribution of the CNM.

DETERMINATION OF MODEL

The authors have already introduced higher and lower order fits, *i.e.*, quadratic and zeroth, to improve accuracy and availability of the correction information, respectively [6]. Both RCM and CNM could determine which model should be used for fit with a given geometry to achieve lower residual error.

Quadratic Model

In the low magnetic latitude region, the spatial distribution of ionospheric delays may not be modeled properly by a planar model. There are usually equatorial anomaly and/or large-scale structures not fit to the first order plane. Figure 6 also gives an example that quadratic fit might be adequate.

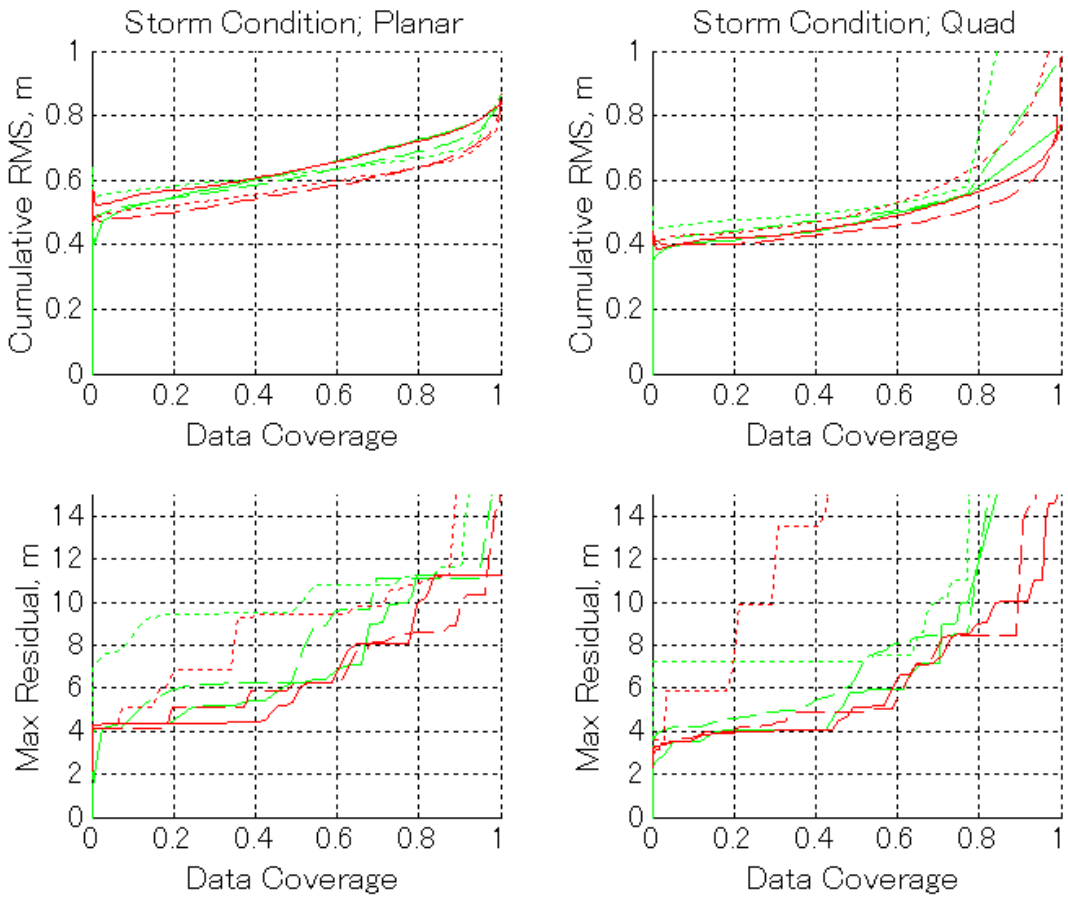

Figure 9. Residual error versus threshold of the metrics, RCM (Red) and CNM (Green), during severe storms. Planar or quadratic fits are performed if the associate metric is less than the threshold. Note that both horizontal and vertical axes mean cumulative values, and the metrics are indicated through the coverage of data. Solid, broken, and dotted lines represent cases of $N_{min} = N_{max} = 30$, 20, and 10, respectively.

Quadratic fit requires 6 parameters to be estimated instead of 3 for planar fit. This means that quadratic fit lowers the degree of freedom in order to estimate additional 3 parameters, so there is a tradeoff relationship between degree of freedom and the order of fit. We need to determine which model is better for each IGP without true measurement. This decision shall be made based on the geometry of IPPs along our approach.

Note that user receiver algorithms do not need to change even in case that SBAS MCS employs quadratic fit to estimate vertical ionospheric delay at an IGP. Changing a model of ionosphere here influences only estimation process in the MCS. User receivers should still compute corrections with the standard bilinear interpolation defined by SARPs [2].

Figure 9 gives an evidence to determine the order of fit. The RMS and the maximum of residual errors are plotted with respect to the threshold of geometry monitor metrics. Both horizontal and vertical axes mean cumulative values. Data coverage means the number of IGPs whose metric is less than the associate threshold divided by the number of whole IGPs; For example, data coverage of 0.5 means the threshold such that planar fit is performed for 50% of IGPs with metrics smaller than the threshold. Solid, broken, and dotted lines represent cases of *Nmin* = *Nmax* = 30, 20, and 10, respectively. Note that even CNM will differ from each other for the different number of observations, with horizontal axis of data coverage we can compare the performance of each case directly.

It can be said that there are the thresholds for RCM and CNM that quadratic fit can provide smaller residual errors than planar fit does for 80% of IGPs. But above the thresholds, residual error possibly becomes large.

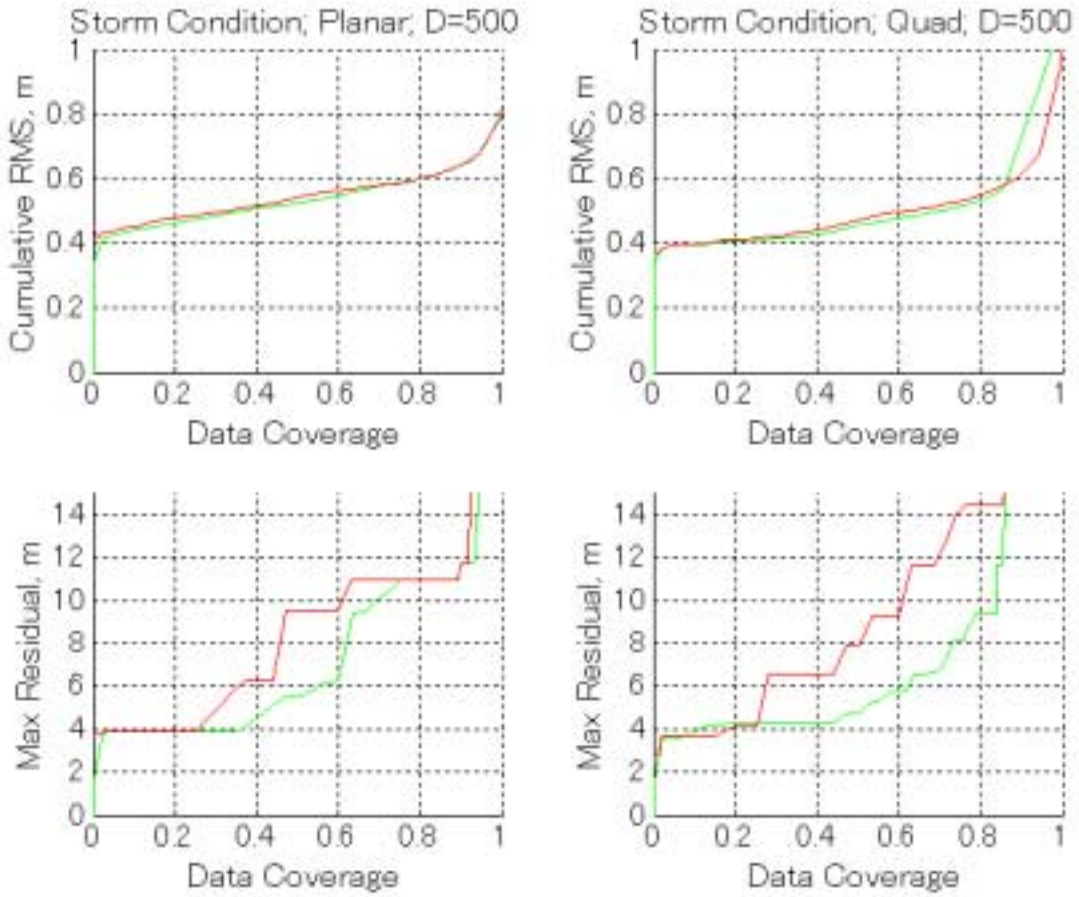

Figure 10. Residual error versus threshold of geometry monitor metrics during severe storms with space constant of D=500 km. Planar or quadratic fits are performed if the associate RCM (Red) or CNM (Green) is less than the threshold.

Quadratic fit reduces the largest error for cases of N>20, but otherwise, the largest error also becomes large due to insufficient degree of freedom.

Decreasing the Number of Observations

In case such that the spatial distribution of ionospheric delays is as displayed in Figure 6, there are cases that the fit radius should not become large. For such a condition, the MCS might decrease the number of IPPs used for fit to improve the estimation performance. However, Figure 9 implies that one should use more IPPs to avoid a large residual error which cannot be bounded by GIVE value.

There is another way to decrease observations effectively. Deweighting observations based on the distance from the IGP reduces the effective fit radius. IPPs far from IGP have smaller weights so that the estimation depends more upon IPPs near the IGP. If there are less observations near the IGP, the weights of outer observations increase relatively so the effective number of IPPs is maintained at a certain level.

To deweight an observation, simply it is necessary to decrease the diagonal components of matrix W. Here we deweight the observation exponentially to the distance:

$$w'_{ii} = w_{ii} \cdot e^{-d_i / D}, \qquad (7)$$

where d_i is the distance between IPP and IGP, and D is a space constant. For non-diagonal components of W, similarly,

$$w'_{ij} = w_{ij} \cdot e^{-(d_i + d_j) / 2D}, \qquad (7)$$

might be employed.

Figure 10 shows the relationship between residual errors and the metrics computed for D = 500 km during October 2003 and November 2004 storms. Comparing with Figure 9, large residual errors with less number of observations are eliminated. For the first order fit, RMS of residual errors is reduced with any N; This fact means that there are structures with the spatial scale smaller than the maximum radius R_{max} = 2100 km. There is a certain threshold of the CNM for quadratic fit which bounds residual errors up to 6 meters and provides RMS residual better than planar fit does both for 60 % of IGPs.

The authors would like to note that Kriging algorithm developed in the field of geostatistics actually has a kind of mechanism similar to this deweighting. Kriging provides the estimation of a plane with the optimal weighting to the observations based on the variogram of the observations, which mathematically equals to covariance function. With the variogram computed dynamically from realtime observations, Kriging implicitly changes fit radius adaptively. This is the optimal estimation theoretically, however, unfortunately cannot overcome undersampling effects; In order to avoid integrity break due to undersampling, we cannot depend upon the realtime observations. In this context, Kriging should be performed with stationary variogram based on the worst storm condition.

Applying Zeroth Fit for Poor Geometry

Based on Figure 10, the MCS can determine the order of fit to improve RMS performance, with protecting users against the largest residual error observed historically. If the geometry of IPPs is good enough, quadratic fit gives the best performance. Otherwise planar fit will be chosen. But, at least for 10% of IGPs, planar fit cannot bound the largest residual error greater than 12 meters. We still must protect users from such conditions by giving up doing planar fit; We should yet decrease the order of fit and keep degree of freedom.

As the authors previously reported, the zeroth order fit can be performed in case that the number of IPPs is insufficient in order to improve availability of the ionospheric corrections [6]. The zeroth order fit means actually simple weighted average so this is robust estimation. For poor geometry with CNM not enough to perform planar fit, even if the number of IPPs is sufficient, we should switch to zeroth order fit and avoid a large residual error introducing integrity break.

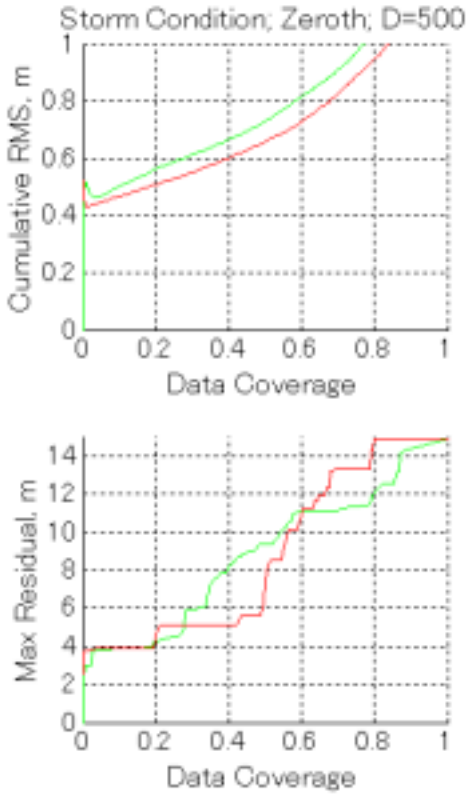

Figure 11. Residual error versus threshold of geometry monitor metrics for zeroth fit. Metrics plotted here are (Green) fit radius metric; and (Red) distance to centroid metric.

For zeroth order fit, CNM is not defined because for such a case there is only one singular value. Uncertainty introduced by zeroth fit depends upon the distance to the IPPs due to the first order component that zeroth order fit cannot remove, so RCM is also not adequate to describe the geometry for zeroth fit.

For these reason, Figure 11 illustrates residual errors of zeroth fit with respect to the fit radius metric (FRM) and the distance to centroid metric (DCM) instead of CNM and RCM. FRM means the largest distance to the IPP used for fit while DCM is the distance to the weighted centroid, i.e., these are the denominator and the numerator of RCM, respectively. During severe storms, DCM gives performance better than FRM. DCM can bound residual errors up to 6 meters for 50% of IGPs and the largest was 15 meters.

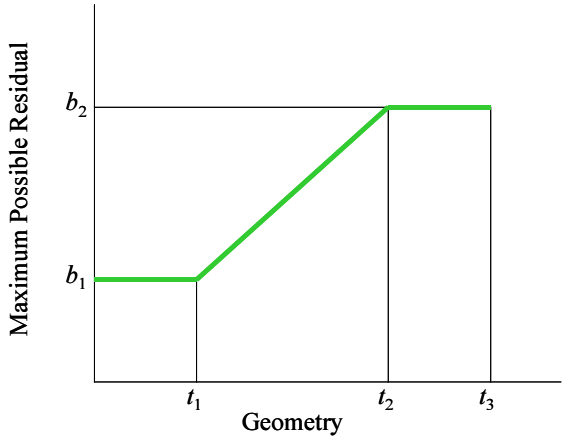

Figure 12. Proposed bounding function for the adaptive fit algorithm. If the geometry is greater than the threshold t_3, such a fit will not be performed.

ADAPTIVE FIT PROCEDURE

Now we have three models to fit ionosphere and the associate geometry monitor metrics to measure the goodness of geometry. Our goal here is implementing the adaptive fit algorithm based on the geometry. First, it is necessary to consider of bounding function.

Even without the assumption that the distribution of residual error is normal, residual error still must be bounded by broadcast GIVE values. One possible way to set GIVE values properly is using a maximum possible residual involved in historical observations during storm conditions. For this approach, it is necessary to find an appropriate function providing the upper bound of residual errors. The geometry monitor metrics introduced above sections have a certain relationship to the largest residual error, so we can construct bounding functions based on such metrics.

According to Figure 10 and 11, the authors would like to propose the form of bounding function as illustrated in Figure 12. The function is proportional to the metric, m, and bounded by b_1 and b_2. If the metric is greater than the threshold t_3, the fit should not be performed because the residual error possibly becomes very large.

Bounding parameters are listed in Table 1 for this simple function. Percentage in the blankets below thresholds means the ratio of IGPs with the metric less than the threshold during October 2003 and November 2004 storms. Parameters in Table 1 is determined based on these severe storms.

Table 1. Parameters of Bounding Functions.

#	Model	Metric	t_1	t_2	t_3	b_1	b_2
1	Quad	CNM	55 (28%)	180 (77%)	250 (83%)	4.4	9.4
2	Planar	RCM	0.41 (38%)	0.43 (46%)	0.45 (53%)	11	12
3	Planar	CNM	18 (12%)	23 (33%)	23 (33%)	9.2	20
4	Zeroth	FRM	1600 (8%)	2000 (58%)	- (100%)	9.1	15

Adaptive fit procedure based on the geometry monitor metric is as follows:

1. Compute a geometry monitor metric for the order of fit.

2. If the metric is smaller than the threshold t_3, employ resulted estimation and set bounding information as a function of the metric, m,

$$5.33\sigma_{bound,IGP}(m) = \begin{cases} b_1, & m < t_1 \\ (b_2 - b_1)\dfrac{m - t_1}{t_2 - t_1} + b_1, & t_1 < m < t_2 \\ b_2, & t_2 < m \end{cases}, \quad (8)$$

3. Otherwise, i.e., if the metric is greater than t_3, try the next model.

Following this procedure from the second to the zeroth order, the MCS can determine an allowable order for fit with a given distribution of IPPs. The associate bounding function can also be computed by Eqn. (8) which becomes the source of GIVE value.

Note that by this approach bounding information is set to protect users from all cases of historical severe storms involved to the definition of bounding functions. In fact, integrity might be broken by a storm condition such that we have never encountered, but, at least, this approach can protect users from all observed storms without missed detection conditions.

Table 2. Comparison of Fit Performance.

Period	Condition	Standard Planar Fit					Proposed Adaptive Fit			
		Storm Detector	RMS residual	RMS σ_{bound}	Max $\Delta_{v,IGP}$	Availa-bility	RMS residual	RMS σ_{bound}	Max $\Delta_{v,IGP}$	Availa-bility
04/11/8-10	Severe storm	Applied	0.566 m	1.305 m	5.082	73.1%	0.577 m	1.295 m	5.105	73.1%
		No	-	-	-	-	0.841 m	1.316 m	5.326	99.4%
03/10/29-31	Severe storm	Applied	0.593 m	1.338 m	5.717	82.1%	0.768 m	1.421 m	5.326	82.1%
		No	-	-	-	-	1.045 m	1.435 m	5.326	99.1%
04/6/22-24	Quiet	Applied	0.328 m	1.265 m	1.825	99.5%	0.311 m	1.319 m	2.421	99.5%
		No	-	-	-	-	0.311 m	1.319 m	2.421	99.5%
04/7/22-24	Active	Applied	0.345 m	1.267 m	1.945	99.2%	0.338 m	1.310 m	2.112	99.2%
		No	-	-	-	-	0.340 m	1.310 m	2.278	99.5%

Performance Evaluation

In order to evaluate the performance of adaptive fit algorithm, it was tested for some periods and ionospheric conditions. The standard planar fit with the chi-square storm detector was also considered for comparison.

Firstly the standard planar fit achieves the following overall performance. During severe storms, the availability of ionospheric corrections lowers to 70-80% due to trip of storm detector. RMS of residual errors, which represents the correction accuracy of the system, varied 0.3-0.4 meter nominal conditions while 0.5-0.6 meter for severe storms. RMS of bounding information, σ_{bound}, was about 1.3 meters regardless of ionospheric conditions. However, the normalized residual error, $\Delta_{v,IGP}$, often exceeds 5.33 that means breaking 10^{-7} level of integrity.

On the other hand, the adaptive fit algorithm achieves the availability of the ionospheric corrections over 99% (lower lines for each period on the table). The normalized residual is bounded by 5.33 while σ_{bound} increased slightly up to 0.1 meter.

For the common set of IGPs that standard planar fit could be performed without trip of storm detector (upper lines), both the normalized residual errors are similar to those of the standard planar fit except during October 2003 storm. This fact means that the proposed adaptive fit algorithm will at least maintain the similar level of correction accuracy while eliminating missed detection conditions which threatens integrity of the system.

For the nominal conditions, the adaptive fit algorithm bounded large residual errors with a slight increase of σ_{bound} up to 0.06 meter, without changing the parameters set based on severe storm conditions.

CONCLUDING REMARKS

The authors introduced geometry monitor concept to overcome undersampling threat. Using an appropriate metric indicating goodness of the geometry of observations, it is possible to bound the actual errors by a function of the metric, as well as determine model for fit. Relative Centroid Metric (RCM) and Condition Number Metric (CNM) were evaluated for this purpose.

Employing an adaptive fit algorithm based on the geometry monitor, the availability of the ionospheric corrections improved from 70-80% to over 99%. Missed detection conditions are eliminated with little enlargement of GIVE values.

Further investigations should include: trying other metrics to improve correction accuracy and GIVE values of the adaptive fit algorithm; considering of temporal variations of ionosphere; and studying scintillation effects.

Following the failure of MTSAT-1 launch in 1999, MTSAT-1R geostationary satellite was successfully launched in February. It is now under test procedures and will broadcast test signals soon. The MSAS program is reaching to a milestone going on the operational phase.

REFERENCES

[1] J. Imamura, MSAS Program and Overview, *Proc. 4th CGSIC IISC Asia Pacific Rim Meeting*, 2003 Joint Int'l Conference on GPS/GNSS, Tokyo, Nov. 2003.
[2] *International Standards and Recommended Practices, Aeronautical Telecommunications*, Annex 10 to the Convention on International Civil Aviation, vol. I, ICAO, Nov. 2002.
[3] *Minimum Operational Performance Standards for Global Positioning System/Wide Area Augmentation System Airborne Equipment*, DO-229C, RTCA, Nov. 2001.
[4] A. Komjathy, L. Sparks, A. Mannucci, and X. Pi, An Assessment of the Current WAAS Ionospheric Correction Algorithm in the South American Region, *Navigation: J.*

Institute of Navigation, vol. 50, no. 3, pp. 193-204, Fall 2003.
[5] T. Sakai, K. Matsunaga, K. Hoshinoo, T. Walter, Evaluating Ionospheric Effects on SBAS in the Low Magnetic Latitude Region, *Proc. 17th Int'l Tech. Meeting of the Satellite Division of the Institute of Navigation (ION GNSS)*, pp. 1318-1328, Long Beach, CA, Sept. 2004.
[6] T. Sakai, K. Matsunaga, K. Hoshinoo, T. Walter, Improving Availability of Ionospheric Corrections in the Low Magnetic Latitude Region, *Proc. ION National Technical Meeting*, pp. 569-579, San Diego, CA, Jan. 2005.
[7] T. Yoshihara, T. Sakai, N. Fujii, and A. Saitoh, An Investigation of Local-scale Spatial Gradient of Ionospheric Delay Using the Nation-wide GPS Network Data in Japan, to be presented in the ION National Technical Meeting, San Diego, CA, Jan. 2005.
[8] P. Doherty, S. Delay, C. Valladares, and J. Klobuchar, Ionospheric Scintillation Effects on GPS in the Equatorial and Auroral Regions, *Navigation: J. Institute of Navigation*, vol. 50, no. 4, pp. 235-245, Winter 2003-2004.
[9] K. Matsunaga, K. Hoshinoo, and K. Igarashi, Observations of Ionospheric Scintillation on GPS Signals in Japan, *Navigation: J. Institute of Navigation*, vol. 50, no. 1, pp. 1-7, Spring 2003.
[10] A. Saito, Y. Otsuka, T. Tsugawa, K. Matsunaga, and K. Hoshinoo, Ionospheric Variations at Midlatitide Detected by a Dense GPS Receiver Array in Japan, *Proc. ION 61st Annual Meeting*, Boston, MA, June 2005.
[11] T. Walter, A. Hansen, J. Blanch, P. Enge, T. Mannucci, X. Pi, L. Sparks, B. IIjima, B. El-Arini, R. Lejeune, M. Hagen, E. Altshuler, R. Fries, and A. Chu, Robust Detection of Ionospheric Irregularities, *Proc. 13th Int'l Tech. Meeting of the Satellite Division of the Institute of Navigation (ION GPS)*, pp. 209-218, Salt Lake City, UT, Sept. 2000.
[12] David S. Coco, Clayton Coker, Scott R. Dahlke, and James R. Clynch, Variability of GPS satellite differential group delay biases, *IEEE Trans. Aerospace and Electronics Systems*, vol. 27, no. 6, pp. 931-938, Nov. 1991.
[13] Brian D. Wilson, Colleen H. Yinger, William A. Feess, and Chris Shank, New and Improved: The Broadcast Interfrequency Biases, *GPS World*, pp. 56-66, Sept. 1999.
[14] H. Konno, S. Pullen, M. Luo, and P. Enge, Analysis of Ionosphere Gradient Using Japan GEONET Data, *Proc. ION National Technical Meeting*, pp. 1118-1129, San Diego, CA, Jan. 2005.
[15] E. Altshuler, D. Cormier, and H. Go, Improvements to the WAAS Ionospheric Algorithms, *Proc. 15th Int'l Tech. Meeting of the Satellite Division of the Institute of Navigation (ION GPS)*, pp. 2256-2261, Portland, OR, Sept. 2002.